SLAC-PUB-8950
LCLS-TN-01-7
August 2001

A Sub-Picosecond Photon Pulse Facility for SLAC*

M. Cornacchia[a], J. Arthur[a], L. Bentson[b], R. Carr[a], P. Emma[b], J. Galayda[a, b], P. Krejcik[b],
I. Lindau[a], J. Safranek[a], J. Schmerge[a], J. Stohr[a], R. Tatchyn[a], A. Wootton[c]

Introduction

It is possible to generate very bright sub-picosecond pulses of spontaneous x-ray radiation utilizing the electron beam from the SLAC linear accelerator and an undulator. The present injection-damping ring system used to inject into the PEP-II B-Factory can be used for this purpose, without any modification to the linear accelerator except for a sequence of 4 bending magnets to compress the electron bunch. With a charge of 3.4 nC per bunch accelerated to 28 GeV and a 10 m long undulator it is quite feasible to generate pulses of x-rays of 8.3 kV energy (in a spectrum extending to over 1 MeV), 80 fsec long (full-width-half-maximum), with a peak brightness of the order of 10^{25} photons/(sec×mm^2 ×mrad^2×0.1% bandwidth), and 10^8 photons per pulse in a 0.1% bandwidth.

This facility could be built and operated ahead of the LCLS schedule and would provide both a powerful tool for research in its own right, as well as a way to conduct critical accelerator and x-ray optics R&D for the LCLS.

This proposal envisions electron bunch compression in three stages, starting with the existing damping ring bunch compressor (Ring-To-Linac section, RTL). A second stage of compression is added in the form of a simple magnetic chicane installed at the 9-GeV location in the linac. A third compression stage is the existing Final Focus Test Beam (FFTB) beamline where a bunch length of 80 fsec (full-width-half-maximum, fwhm) at 28 GeV is produced. A new 10-m long undulator located here produces intense spontaneous x-ray radiation, which is transported to an experimental hutch, placed outside the FFTB area. The FFTB hall, in terms of its size and infrastructure (mechanical and temperature stability), is very suitable for setting up such a source.

This paper is organized as follows:
- Section 1: Layout of the facility and main performance parameters.
- Section 2: Scientific opportunities and LCLS-directed R&D.
- Section 3: Physics and engineering aspects of electron bunch compression.
- Section 4: The undulator and its electron optics.
- Section 5: The characteristics of the spontaneous radiation emitted by the undulator.
- Section 6: Take-off x-ray optics and experimental area.
- Section 7: Cost and construction schedule.

The concept of using the SLAC linac to generate radiation from an undulator has evolved from several earlier proposals[1,2,3,4]

[a] Stanford Synchrotron Radiation Laboratory, a division of Stanford Linear Accelerator Center
[b] Technical Division, Stanford Linear Accelerator Center
[c] Lawrence Livermore National Laboratory
[1] P.H. Fuoss, NIM A264, 497 (1988).
[2] J. Seeman, R. Holtzapple, "An 'NLC-Style' Short Bunch Length Compressor in the SLAC Linac", SLAC-PUB-6201 (1993).
[3] P. Emma, J. Frisch, "A Proposal for Femtosecond X-ray Generation in the SLC Collider Arcs", SLAC-PUB-8308 (1999).
[4] P. Krejcik, "Parameters for a 30 GeV Undulator Test Facility in the FFTB/LCLS", SLAC-PUB-8806 (2001).

1. General layout and projected performance

The general layout of the facility is shown in **Figure 1**.

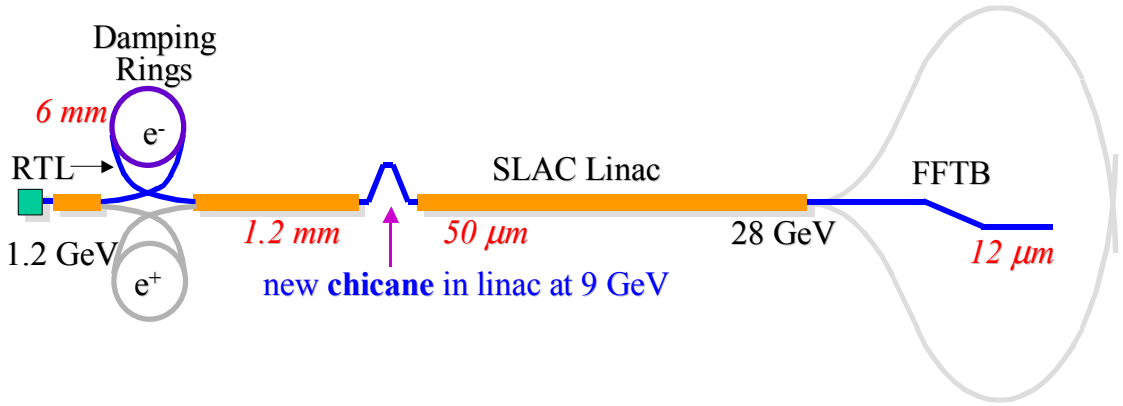

Figure 1. Layout of the SPPS in the SLAC accelerator complex. The root-mean-square bunch length (rms) is shown at various stages.

A single electron bunch with 2.2×10^{10} electrons is extracted from the North Damping Ring, as is currently done for injection into the PEP-II storage ring. With reference to **Figure 1**, the electron bunch compression will be done in three stages, starting with the existing Ring-To-Linac (RTL) compressor at the exit of the damping rings, where the bunch length is compressed from 20 psec (6 mm) to 4 psec (1.2 mm) - rms values. A second stage of compression requires the addition of a new magnetic chicane to the linac at the 9 GeV location, which compresses the bunch down to 160 fsec rms (50 μm). The third stage of compression occurs in the bends of the present FFTB beamline, which produce a 35 fsec rms bunch length (12 μm) at 28 GeV (80 fsec fwhm). A 10 m long undulator in the FFTB generates spontaneous radiation at the undulator fundamental photon energy of 8.3 keV and extending to over 1 MeV. The radiation is transported to an experimental area placed outside the FFTB. **Table 1** lists the main characteristics of the spontaneous radiation and of the electron beam at the undulator.

Table 1. Main SPPS radiation (8.3 keV) and electron beam (28 GeV) parameters

Peak photon brightness	9.1×10^{24}	photons/(sec×mm^2×mrad^2×0.1% bw)
Pulse length	80	fsec, fwhm
Average photon brightness	2.2×10^{13}	photons/(sec×mm^2×mrad^2×0.1% bw)
Average flux	3.1×10^{9}	ph/(sec×0.1% bw), integrated over all angles

Photons/pulse	1.0×10^{8}	In a 0.1% bw, integrated over all angles
Bunch repetition rate	30	Hz
Charge per bunch	3.4	nC
Energy	28	GeV
Horizontal e^- emittance (rms)	$9.1x10^{-10}$	m-rad
Vertical e^- emittance (rms)	$1.8x10^{-10}$	m-rad

2. Scientific opportunities and LCLS R&D

The most exciting feature of the SPPS will be its combination of synchrotron radiation brightness with sub-picosecond pulse length. This combination will allow the powerful techniques of x-ray diffraction and x-ray absorption spectroscopy to be used to study fast dynamics at the atomic level. Sub-psec dynamics are typically studied in pump-probe fashion, using a femtosecond optical laser as pump. Probe techniques in use today include optical laser spectroscopy[5], electron diffraction[6], x-ray diffraction[7], and x-ray absorption spectroscopy[8].

Of these techniques, laser spectroscopy has been by far the most useful, because of the ready availability of tunable, intense, fsec lasers. However, due to its long wavelength, a laser cannot directly give structural information on an atomic scale. Atomic structure must be deduced indirectly from spectroscopy of the outer electron levels. For complicated structures, this becomes impossible, and a direct structural measurement through diffraction or core-level spectroscopy is needed. Electron and x-ray diffraction can both determine structures, but these methods are difficult to use in the sub-psec range. Sources for electron diffraction are intense, but the time resolution is limited by the difficulty in making sub-psec low-energy electron pulses. Specialized x-ray sources such as laser-induced plasmas can be very fast, but their low brightness is a severe limitation on their utility.

In **Table 2** the SPPS performance is compared with some existing and proposed sub-psec x-ray facilities: the Ultrafast X-Ray Facility at the Advanced Light Source, the proposed re-circulating linac light source

[5] *Femtochemistry and Femtobiology: Ultrafast Reaction Dynamics at Atomic Scale Resolution*, V. Sandstroem, ed., World Scientific, Singapore 1997.
[6] H. Ihee, et al., Science **291**, 458 (2001).
[7] R. W. Schoenlein, et al., Science **287**, 2237 (2000).
[8] C. P. J. Barty, et al., in *Time-Resolved Diffraction*, J. Helliwell and P.M. Rentzepis, eds., Oxford Univ. Press, New York 1998, p. 44.

(ERL) at LBNL, and the projected LCLS Free-Electron Laser. These are all facilities capable of delivering bunches of the order of 100-200 fsec long. In this table the SPPS undulator is optimized for 1.5 Å radiation. As it will be discussed in Section 6, undulators covering different wavelength ranges are also possible. The final choice of undulator remains to be made, and will be based largely on the requirements of the experiments.

Table 2. Radiation characteristics of the SPPS and other ultra-fast x-ray facilities.

Facilities	Peak brightness*	Pulse length (fwhm, fsec)	Average brightness *	Average flux (ph/s, 0.1%-bw)	Photons/pulse 0.1%-bw	Rep. rate (Hz)
SLAC SPPS	9.1×10^{24}	80	2.2×10^{13}	3.1×10^{9}	1.0×10^{8}	30
ALS Ultrafast Fac.(undulator)[9]	6×10^{19}	100	6×10^{10}	3×10^{6}	300	1×10^{4}
LBNL ERL[10]	1.0×10^{23}	100	1×10^{14}	2×10^{10}	2.0×10^{6}	1×10^{4}
LCLS FEL[11]	1.5×10^{33}	230	4.2×10^{22}	2×10^{14}	1.7×10^{12}	120

* photons/sec/mm^2/mrad^2/0.1%-bandwidth

The peak brightness of SPPS will exceed that of any existing hard x-ray source by several orders of magnitude, and its pulse length of <100 fsec will allow it to explore the same time correlations as the fastest existing or proposed sources. The brightness of SPPS will greatly expand the practical range of sub-psec x-ray diffraction experiments. Where current experiments are limited to high-reflectivity perfect crystals, the SPPS would allow the use of weaker reflections and powder diffraction. This would allow studies of a wide variety of phase transitions and chemical reactions in solids. While SPPS could not support diffraction from very weakly-scattering samples such as gases and biological crystals, core-level x-ray spectroscopy (NEXAFS and EXAFS) could be used to provide some atomic structural information. For most experiments it will be necessary to accumulate data over many pulses, using reversible reactions or reactions in which the reactants can be replenished. The 30Hz repetition rate of SPPS is particularly favorable for this kind of stroboscopic experiment, since it matches well with the repetition rates of fsec pump lasers.

Table 2 lists the expected properties of the LCLS x-ray FEL source, which should be constructed at SLAC in a few years. This source and the other linac-based x-ray facilities that follow will soon revolutionize the field of fast time-resolved x-ray science[12]. However, there is much to be learned about performing sub-psec x-ray experiments properly. The SPPS should prove to be a valuable tool for developing ultrafast x-ray techniques. Areas that require R&D include:

Synchronization. The synchronization of an optical pump laser with an x-ray source at the sub-psec level will be challenging. Even measuring the time correlation of two such disparate pulses with precision below 100 fsec will require exploiting and developing novel nonlinear x-ray effects.

[9] Schoenlein and others, "Generation of femtosecond x-ray pulses via laser-electron beam interaction", Appl. Phys. B 71, 1-10 (2000), Table 1

[10] A. Zholents, "On the possibility of a femtosecond x-ray pulse source vased on a recirculator linac", CBP Tech Note-210, Nov. 14, 2000.

[11] LCLS Design Study Report, SLAC-R-521 (1998).

[12] LCLS: The First Experiments, G. Shenoy and J. Stohr, eds., SSRL 2000.

Temporal stability. Light travels only 30 μm in 100 fsec. Experiments must be carefully designed to eliminate path length variations that could affect the time resolution. Also, the effects on x-ray pulse length of standard x-ray optical elements such as monochromators are not entirely understood.

Efficient detectors. Both ultrafast detectors such as streak cameras and large-area time-integrating detectors will be useful for SPPS experiments.

Although the main objective of this source of ultra-short pulses is to produce exciting science for those experiments that can use high peak-brightness and photon flux, and <100 fsec long pulses, important R&D, critical to the LCLS and x-ray FELs in general, could be conducted with a tool that would have no equal in the world in terms of short pulses, peak brightness, and photon flux. Major advances could be made in accelerator and FEL physics and x-ray optics with this source.

- Accelerator physics R&D

a) *Confirmation of the Longitudinal Wakefield for an Extremely Short Bunch*
The longitudinal geometric wakefield of the SLAC S-band RF structures has been measured many times using an electron bunch typically 3 psec in rms length. The LCLS beam will eventually be compressed to a length of <100 fsec and the subsequent longitudinal wakefield induced by 500 meters of accelerating structures is critically used to suppress the final energy spread to a level of <0.1%. The control of this suppression is dependent on a thorough understanding of the wakefield induced by this micro bunch. The SPPS configuration transports a 160 fsec bunch length through 1.9 km of RF structures. The final energy spread of 1.5% (rms) is completely dependent on the wakefield and will provide an essential measurement to confirm the LCLS design.

b) Emittance Growth in a Compressor Chicane
The bend-plane emittance is not preserved in a chicane bunch compressor. Dilution mechanisms include the effects of coherent and incoherent synchrotron radiation, inadequate field quality in the dipole magnets, and longitudinal wakefields induced by the vacuum chamber. Limited experience and understanding is available at present, especially in conjunction with an extremely short bunch length. The SPPS chicane will offer the opportunity to confirm emittance preservation on a scale which is similar to that of the LCLS. The SPPS will be the first facility in the world where coherent synchrotron radiation effects can be studied at such high energy. Wire scanners for emittance measurement already exist in the linac just downstream of the proposed chicane location.

c) Bunch Length diagnostics and feedback
The micro-bunch after compression will need to be measured with adequate precision to tune-up and to continually stabilize the LCLS beam. One method planned for the LCLS uses a transverse RF deflector to 'streak' the bunch onto a profile monitor. Such an RF deflector is already installed downstream of the proposed SPPS chicane and can be fully tested. In addition, other micro-bunch radiation monitors could be tested and calibrated against the absolute bunch length measured by the transverse rf deflector.

d) RF Phase and Voltage Stability
The RF phase and voltage stability tolerances for the LCLS linac are quite challenging, based as they are at the levels of 0.1° and 0.1%, respectively. Existing RF stability measurements are not beam-based and are therefore not conclusive with adequate precision. Bunch compression in the SPPS chicane requires similar RF stability and will afford the opportunity

to confirm stability on the same machine as will be used to support the LCLS. Other schemes for tuning and stabilizing the RF in the LCLS can be tested and developed at the SPPS.

e) *Preservation of Electron Beam Brightness through the Existing BSY and FFTB*
The bunch will pass through some of the very same vacuum chambers, which will be used to transport the LCLS beam. This includes the FFTB, and the beam switchyard area where the vacuum chambers are large, but vary in aperture with some complexity. A demonstration of beam brightness preservation through these same sources of impedance will form a solid base to support the LCLS design.

- X-Ray Optics R&D

This facility would bring major progress in crucial areas of the x-ray optics R&D. These are: development of x-ray components, photon diagnostics and study of damage to components.

f) *Developments of x-ray components*
The photon energy, cross section, pulse length and repetition rate are suitable for LCLS research in lenses, zone plates, filters, apertures, beam splitters, etc. While present 3rd generation sources also offer the relevant photon energy, the proposed facility will allow us to understand component response to individual ultra-short pulses. One of the critical functions of the x-ray optical components and instrumentation under development by the X-ray Optics Group is the control and modulation of the LCLS radiation phase space. Two specific examples, relevant both to the FEL Physics and the initial scientific programs proposed for the LCLS, are time slicing and strong focusing. Optical components for both of these functions will be developed and incorporated into the proposed SPPS facility to attain power density and pulse length ranges comparable to or greater than those of the LCLS beam. In this regard, the LCLS X-Ray Optics Group will be involved not only in the end use, but also in the co-development of some of the key technologies on which this facility will be based.

g) *Photon diagnostics*
Here again it is the combination of pulse length, photon energy and cross section of the SPPS facility that will allow, for example, to test our concepts for measuring beam profiles, beam divergence, and beam centroid. It will also allow us to develop diagnostics to measure pulse length at the correct energy, and to research and develop means of measuring the synchronization between an individual x-ray pulse at a few keV and an individual optical pulse at a few eV, in anticipation of pump-probe experiments on the LCLS.

h) *Damage to components*
Concerning the all-important question of damage to components, the present strategy assumes that no deleterious effects will occur on the ~100 fsec timescale, and that longer term (i.e. after the pulse) effects are reversible and thus harmless, as long as the absorbed energy is kept below that required to bring material up to the melting temperature. While these working assumptions are based on theory, they require experimental verification. The SPPS can be used for damage studies at the lower energies (~ 1 keV) for higher Z materials (e.g. Au, Zr, Ir, Cu) if the photon area density can be increased by a factor ~30 to ~100. That is, even allowing for losses in the focusing element, a de-magnification of <10 would be sufficient to allow the proposed facility to be used as a damage test facility for the LCLS, at relevant photon energies, pulse lengths and materials.

i) Production of ultra-short x-ray pulses via time slicing

When operated at full bunch compression, the average temporal structure of the SPPS photon pulses will be similar, both in profile and duration, to the 80 fsec (fwhm) long electron bunches. In addition to this standard mode of operation, it will also be possible to generate ultra-short pulses with a non-compressed electron bunch via the alternative technique of time slicing using multi-layers or crystals, and where the pulse duration and shape is defined by the optics. This is an important area of research for the LCLS that the SPPS could prepare for: it would allow the LCLS to produce photon pulses shorter than the nominal 230 fsec (fwhm). It will also provide an alternative to magnetic compression for the generation of ultra short x-ray pulses in the SPPS.

In the slicing technique[13] the photon pulse with a longitudinal monotonic wavelength chirp $\Delta\lambda_{0N}(=\lambda_0 - \lambda_N)$ and total length L is made to intercept a multi-layer with period d at an incidence angle θ. If some subinterval of the impinging pulse has a mean wavelength λ_i, which satisfies the multilayer Bragg condition ($\lambda_i = 2d\sin\theta$), then that part of the sub-interval that lies within the multilayer's passband, $\Delta\lambda$, will be reflected at an exit angle θ, while the remainder of the pulse will be scattered and absorbed. This process is shown graphically in **Figure 2**.

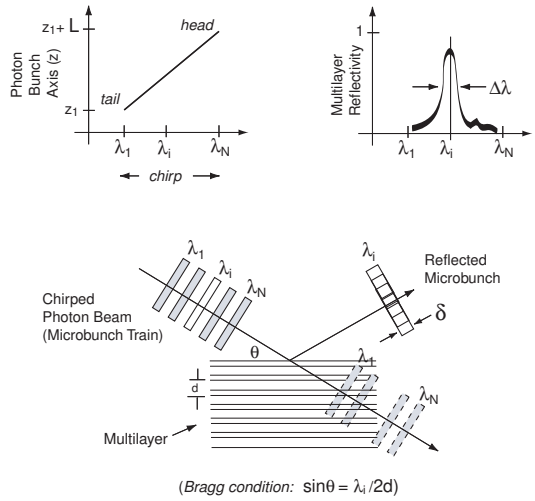

Figure 2. Wavelength chirp and selection with a multi-layer

In this example the bunch is compressed less strongly than in the reference SPPS parameters of **Table 1**. 1.6 psec (fwhm) at the undulator have been assumed, with a 0.9% longitudinally correlated energy spread (rms)[14], compared to the 1.5% of the compressed bunch. A multi-layer optics of suitably designed bandwidth will extract correspondingly short intervals out of the energy chirped photon pulse. The length and detailed temporal structure of these sliced pulses can be readily calculated[15]. Selected performance figures for this mode of ultrashort pulse generation by the SPPS are included in **Table 6**.

[13] R. Tatchyn, "Multilayer-based radiation pulse slicers for Linac Coherent Light Source (LCLS) applications," (2000) LCLS TN-00-17.

[14] Paul Emma, private communication.

[15] R. Tatchyn, R. Bionta, "Performance studies of a multilayer-based radiation pulse slicer for Linac Coherent Light Source applications," SPIE Proceedings 4143, 2001, p. 89.

3. Electron acceleration and compression

The electron beam parameters are largely governed by the boundary conditions of supplying beam to the SPPS parasitically to PEP II operation. The PEP II injection bunches start at the gun and pass through the damping rings and are further accelerated in the high-energy linac. The positron and electron bunches for PEP II are extracted from the linac at the 3 GeV and 9 GeV locations respectively into beamlines that by-pass the rest of the linac. A third electron bunch is accelerated to 25 GeV, where it is extracted and directed to the positron production target. Beyond this extraction point, the last one third of linac is not normally powered. A fourth, "test beam", with a 10 Hz repetition rate, is at times accelerated to the end of the linac in between PEP II injection cycles and directed to the FFTB beamline at the energy of 30 GeV. The damping rings, which operate with a 16.6 ms store time, determine the initial transverse emittance, which is typically $\gamma\varepsilon_{x,y} \approx$ 35x5 mm-mrad (normalized, horizontal x vertical). This value is expected to grow to 50x10 mm-mrad when wake-fields in the linac and the emission of coherent synchrotron radiation in the bends are taken into account.

The shortest achievable final electron bunch length is set by the conservation of longitudinal emittance of the beam. The product of the initial damping ring bunch length, $\sigma_{z_{DR}}$, relative energy spread, $\sigma_{\delta_{DR}}$, and energy, E_{DR}, is, for uncorrelated phase space, equal to the product of the final bunch length, σ_z, final relative energy spread, σ_δ, and final energy, E_f. This leads to the following expression for the minimum final bunch length.

$$\sigma_z = \frac{E_{DR}}{E_f}\frac{\sigma_{\delta_{DR}}\sigma_{z_{DR}}}{\sigma_\delta} \tag{1}$$

The damping ring energy is nominally $E_{DR} \approx 1.19$ GeV, with an rms bunch length of $\sigma_{z_{DR}} \approx 6$ mm, and an rms energy spread of $\sigma_{\delta_{DR}} \approx 0.08\%$ at 2.2×10^{10} e^-/bunch. If the bunch is accelerated to 28 GeV and the final rms energy spread is allowed to increase to $\sigma_\delta \approx 1.5\%$ using wakefields and RF phasing, the minimum achievable bunch length is $\sigma_z \approx 12$ μm rms.

The 6-mm rms bunch length at damping ring extraction is passed through the Ring-to Linac (RTL) beamline where it is compressed down to 1.2 mm (rms). The RTL compressor uses a 2.1 m long section of S-band accelerating structure phased at the zero crossing of the rf field. A gradient of 20 MV/m provides the necessary momentum spread correlated with the position along the bunch. The dependence of path length with momentum ($R_{56} \approx 0.6$ m), generated by the bends in the RTL beamline, compresses the bunch. The idealized compression process is shown schematically in **Figure 3.**

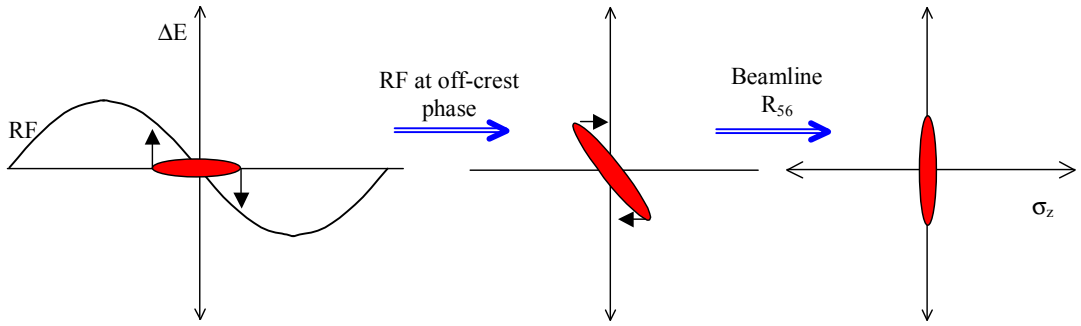

Figure 3. Schematic of ideal bunch compression where the bunch is given a correlated energy spread from head to tail followed by transport through a dispersive section whose path length varies with energy. The vertical axis represents the energy deviation, the horizontal axis the distance along the bunch.

In order to achieve sub-picosecond bunch lengths a second compression stage is required. Accordingly, the second bunch compression should be done at the maximum beam energy to achieve minimum bunch length were it not for the deleterious emittance growth effects of synchrotron radiation in the bends, which increase rapidly with energy. The 9-GeV location is chosen to place the new chicane downstream of the extracted PEP-II beams, which are diverted to by-pass lines on the tunnel ceiling. The linearly correlated energy spread of 1.6% (rms) in the bunch is introduced by accelerating, in the linac sections between the damping ring and the chicane, at an RF phase of –20° from accelerating crest, as shown in **Figure 5d.** This results in a bunch length of approximately 50 μm, or 160 fsec (rms), as shown in **Figure 5e.** The 50 μm electron bunch length, after the chicane, will be measured using the transverse rf deflector presently installed in Sector 29 of the linac[16].

The second bunch compressor takes the form of a magnetic chicane using a simple arrangement of four dipoles to introduce a dispersive path length difference (R_{56}) in the linac. The compressor, shown in **Figure 4**, replicates the design used in the LCLS bunch compression scheme[17]

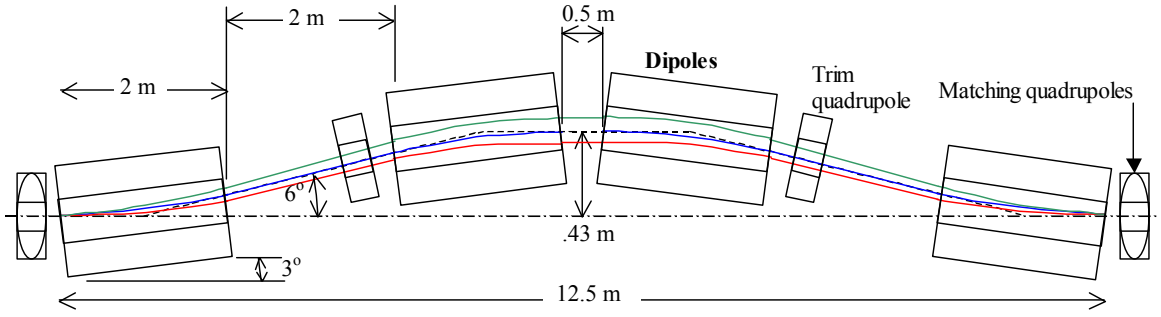

Figure 4. Layout of the magnetic chicane placed at the 9 GeV location of the linac.

The applied RF accelerating voltage is not the only factor affecting the energy distribution along the bunch. At the high peak current considered here the longitudinal wakefield generated by the bunch

[16] R. Akre et al,"A Transverse RF Deflecting Structure` for Bunch Length and Phase Space Diagnostics", presented at the 2001 Particle Accelerator Conference, Chicago, IL, June 2001.
[17] LCLS Design Study Report, SLAC-R-521 (1998)

in the accelerating structure has a strong influence on the final energy distribution. This is best seen by numerically tracking the individual particles through the accelerator[18]. The ideal bunch compression described in equation (1) is only valid if the process remains linear, which is not always the case in presence of strong wakefields. It was found, through computer simulation studies, that the problem of wakefields could be alleviated by shaping the initial charge distribution in the bunch in such way as to over compress[19] the bunch in the first RTL compressor. This is shown in **Figure 5c**. Using a realistic distribution for the bunch extracted from the damping ring[20] it is found that a 41 MV rf amplitude in the RTL gives a 1.2 mm rms bunch length with 3.4 nC of charge and results in the best linear energy distribution along the bunch at the entrance of the chicane compressor at 9 GeV, as shown in **Figure 5d.**

At the exit to the chicane the bunch is compressed to 50 μm and generates even stronger wakefields in the remainder of the linac. This wakefield creates a new energy correlation along the bunch (see **Figure 5f)** that makes it possible to achieve a third compression in the FFTB. On the basis of equation (1) the higher energy of 28 GeV attained at the end of the linac predicts a shorter bunch. A practical limit to the final compression is imposed by the finite energy aperture of the beamline. This sets an upper limit of 1.5% on the rms energy spread of the beam.

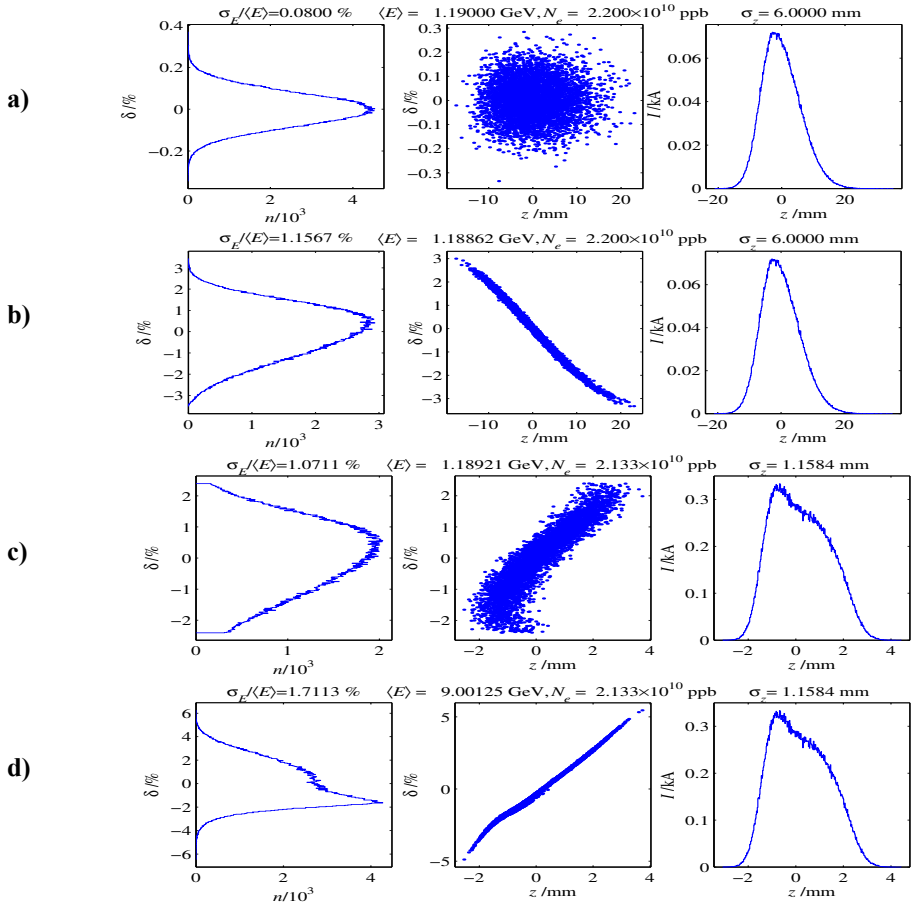

[18] M. Borland, "Elegant: A Flexible SDDS-Compliant Code for Accelerator Simulation", ICAP-2000, Darmstadt, Germany, September 2000.

[19] F.-J. Decker, R. Holtzapple, T. Raubenheimer, "Over-Compression, a Method to Shape the Longitudinal Bunch Distribution for a Reduced Energy Spread" in LINAC94, August 1994.

[20] K. Bane et al., "High-Intensity Single Bunch Instability Behaviour in the New SLC Damping Ring Vacuum Chamber", in ICAP-2000, September 2000.

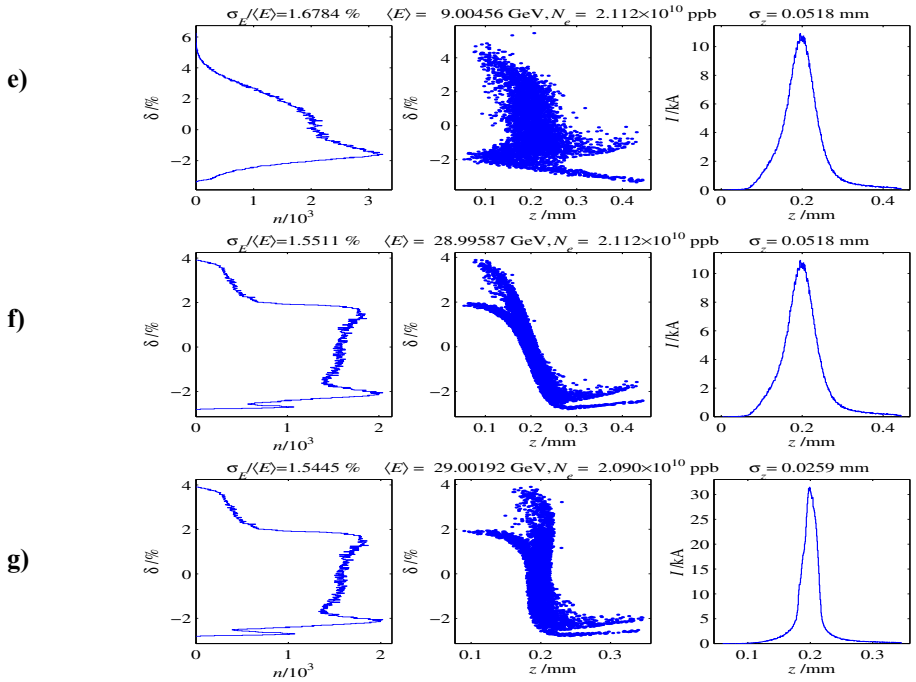

Figure 5. Compression process at various stages. The energy distribution is shown on the left, the phase space distribution is in the center, and the longitudinal distribution is on the right column: a) At damping ring extraction, b) after RTL acceleration, c) after RTL bends, d) at 9 GeV prior to compressor chicane, e) after compressor chicane, f) after linac at FFTB entrance, and g) after FFTB bends. Bunch head toward z < 0.

The existing FFTB beamline generates a small R_{56} term in the, dog-leg bend, which is adequate for the final bunch rotation from 50 μm to 12 μm (rms). The final compressed pulse, shown in **Figure 5g**, has a full-width-half-maximum length of 80 fsec and a peak current of 30 kA. The electron beam properties are summarized in **Table 3**.

Table 3. Main electron beam parameters.

Parameter	*Symbol*	*Value*	*Unit*
Bunch population (after 4% RTL loss)	N	2.1	10^{10}
Damping Ring Energy	E_{DR}	1.19	GeV
Damping ring bunch length (rms)	$\sigma_{z_{DR}}$	6.0	mm
Damping ring energy spread (rms)	$\sigma_{\delta_{DR}}$	0.08	%
Final normalized transverse emittance (rms)	$\gamma\varepsilon_{x,y}$	50, 10	μm
Bunch length after stage 1 (rms)	σ_{z_1}	1.2	mm
Bunch length after stage 2 (rms)	σ_{z_2}	50	μm
Bunch length after stage 3 (rms)	σ_{z_3}	12	μm
Final pulse width, fwhm	$\sigma_{\tau_{min}}$	80	fsec
Final relative correlated energy spread (rms)	σ_δ	1.5	%
Final energy	E_f	28	GeV
Peak bunch current	I_{pk}	30	kA

These parameters have been verified by 6-D particle tracking using the code *Elegant*[21]. The processes of emittance growth due to incoherent (ISR) and coherent synchrotron radiation (CSR) in the various bends have been computed and found to increase the emittance by 15-20%. In the FFTB, the large energy spread requires a new sextupole magnet to be located at the point of largest momentum dispersion. The new 10-cm long sextupole magnet is already available from the SLC final focus where it was never used. With the new sextupole, the remaining chromatic effects increase the emittances by only 2-3 %.

4. The undulator

The choice of photon energy range depends on the electron energy and on the undulator characteristics. If it is assumed that the electron energy is fixed at 28 GeV (to simplify the switch to and from the PEP-II filling energy), then the operational energy range of the photons depends on the undulator. The proposed undulator is a standard asymmetric Halbach hybrid made of NdFeB magnets and vanadium permendur pole-pieces; it is built in 10 segments, each about 1 m long. An internally copper plated stainless steel beampipe, with either circular or oblong cross section, will be inserted in the gap when the segments are assembled.

The undulator will have a gap that is adjustable by manual screw actuation. The parameters are indicated in the table below.

Table 4. Parameters of an undulator optimized for 8.3 keV photon energy

Parameter	*Value (range is for variation of gap)*	*Units*
Period length	45.2	mm
Magnetic gap	8.5 - 12	mm
Resonance energy range - first harmonic	8.26 - 15.5	keV
Vanadium permendur pole dimensions	25 x 25 x 6	mm
NdFeB Magnet dimensions	50 x 50 x 16.6	mm
Remanent field of NdFeB	1.20	T
Segment length	994	mm
Periods per segment	21 full periods, 2 half periods	
Total undulator periods	210 full periods, 20 half periods	
Peak (vertical) magnetic field	1.46 - 1.0	T
Field variation in horizontal ± 0.3 mm central region	0.0022	T
Undulator paramter K	6.15 - 4.32	

[21] M. Borland, "A Simple Method for Simulation of Coherent Synchrotron Radiation in a Tracking Code" in ICAP-2000, September, 2000 .

Photon beam size at sample, 95 m from source	σ_{horz} = 0.72, σ_{vert} = 0.5	mm
Radiation opening angles - first harmonic	θ_{horz} = 7.6, θ_{vert} = 5.2	μrad
Segment straightness to achieve $\Delta E_v/E_v = 0.1\ \Delta E_e/E_e$*	0.075	mm, in horizontal plane
Alignment tolerance achievable over 10 meters	0.150	mm (with conventional methods)
Beam straightness to achieve $\Delta E_v/E_v = 0.1\ \Delta E_e/E_e$	0.3	mm, in horizontal plane
Force between jaws for each segment at minimum gap	10500	N

* Photon energy shift is ≤ 10% of electron energy spread.

The undulator will be constructed of two jaws on individual strong-backs so that the gap between them can be adjusted by jack-screws. Precise gauge blocks will then be inserted between the strong-backs, and the jaws will be allowed to close on the gauge blocks. In order to allow the magnetic measurements, the jaws will be mounted on an external jig, leaving the gap to be open on one side. The structure of the undulator is shown in the figures below:

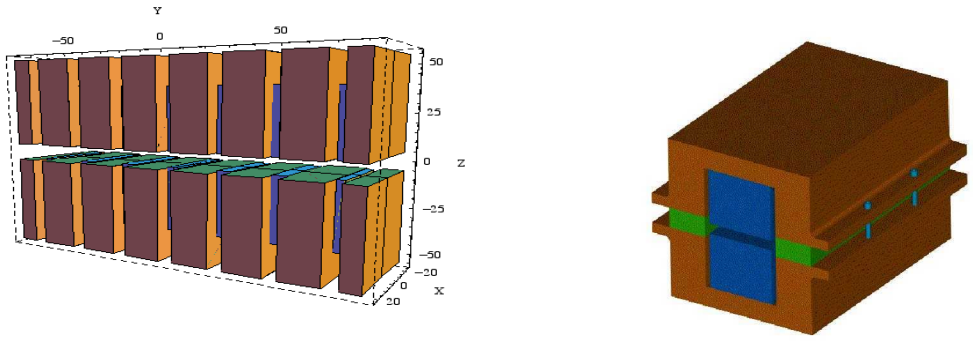

Figure 6. On the left: magnetic structure, with the larger blocks representing the NdFeB magnets and the vanadium permendur poles in between. The end termination is half pole + half magnet. On the right: The mechanical structure end view, with the strong-back frame surrounding the magnetic structure. The screws allow gauge blocks to be placed as spacers.

It is envisaged that trajectory tolerances can be met without any need for trim coils, focusing magnets, or beam position monitors within the undulator. The precise beam control in the FFTB will make it unnecessary to install an upstream collimator to protect the undulator from the electron beam.

The selection of this particular type of undulator does not preclude its replacement with a device optimized for a different part of the spectrum, should the scientific applications require it. For instance, a wiggler could be used for a spectral range extending down to 800 eV.

Electron beam optics in the undulator and beam dump channel

The transverse distribution of the photons is determined by the transverse distribution of the electrons in the undulator. The phase space distribution of photons is the convolution of the electron distribution with the photon opening angle, $\sigma_{r'}$, that would result from a single electron[22]:

$$
\begin{aligned}
&P(x,x') = P_0 \exp\left(-\frac{\gamma_p x^2 + 2\alpha_p x x' + \beta_p x'^2}{2\varepsilon_p}\right) \\
&\alpha_p = \alpha_{e-} / \kappa \qquad\qquad \beta_p = \beta_{e-} / \kappa \\
&\gamma_p = (\gamma_{e-} + \sigma_{r'}^2 / \varepsilon_{e-}) / \kappa \qquad\qquad \varepsilon_p = \kappa \varepsilon_{e-} \\
&\kappa \equiv \sqrt{1 + \sigma_{r'}^2 \beta_{e-} / \varepsilon_{e-}}
\end{aligned}
\tag{2}
$$

Here (α_{e-}, β_{e-}, γ_{e-}, ε_{e-}) are the standard electron optics parameters at the center of the undulator, and (α_p, β_p, γ_p, ε_p) are the analogous parameters for the photon beam.

The two figures of merit for the photon beam distribution are ε_p, the photon emittance, and $\sigma_{p,hutch}$, the photon beam size in the experimental hutch a distance D = 92 meters from the undulator. Minimizing ε_p maximizes the photon beam brightness, while minimizing the photon beam size in the hutch reduces the required size of the photon optics. The photon optics parameters propagated to the hutch give a photon beam size of

$$
\sigma_{p,hutch} = \sqrt{\varepsilon_p (\beta_p - 2\alpha_p D + \gamma_p D^2)}, \qquad \gamma_p = (1 + \alpha_p^2) / \beta_p, \tag{3}
$$

where (α_p, β_p, γ_p) are the photon optics parameters at the undulator. The choice of a slightly converging electron beam at the undulator with $\alpha_{e-} = \beta_{e-}/D$ gives the smallest $\sigma_{p,hutch}$ for a given β_{e-}. For this choice of α_{e-}, **Figures 7 and 8** show ε_p and $\sigma_{p,hutch}$ as a function of β_{e-}.

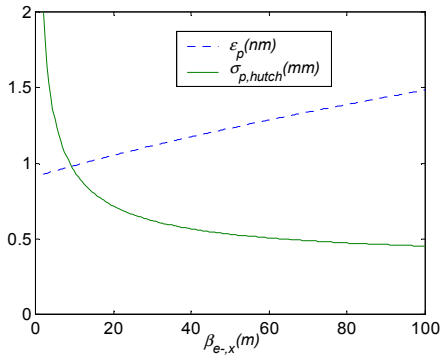

Figure 7 Horizontal photon beam parameters vs. horizontal electron β-function. $\sigma_{p,hutch}$ is for $\alpha_{e-} = \beta_{e-}/D$

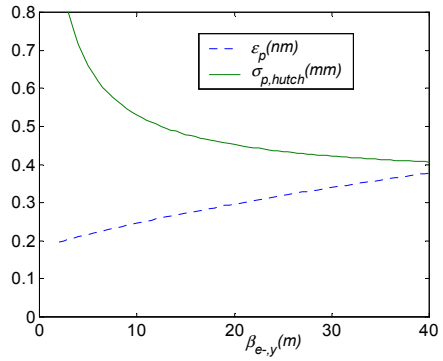

Figure 8 Vertical photon beam parameters vs. vertical electron β-function. $\sigma_{p,hutch}$ is for $\alpha_{e-} = \beta_{e-}/D$.

[22] J. Safranek and P.M. Stefan, "Emittance Measurement at the NSLS X-Ray Ring", BNL-64141 (1996).

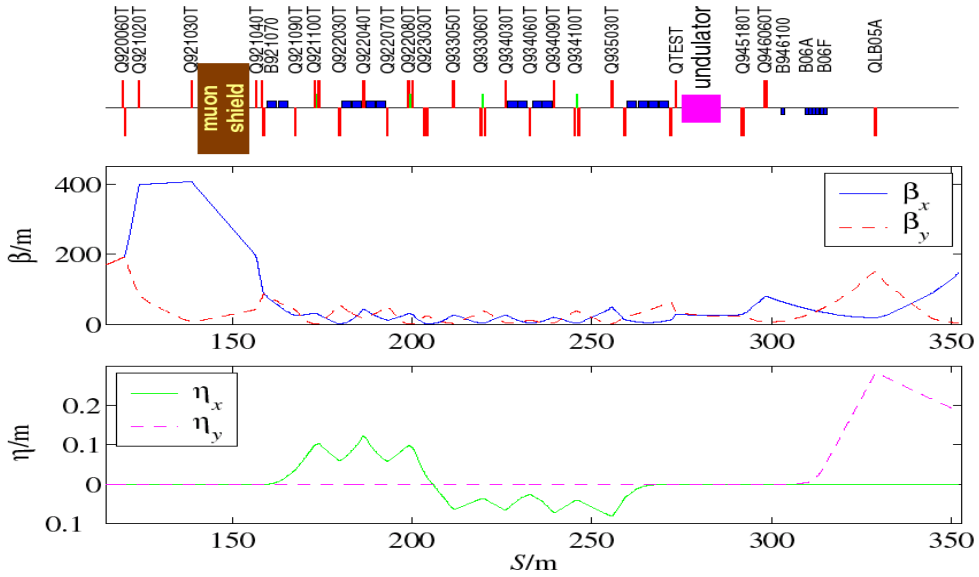

Figure 9. Optics of the electron transport system to the undulator: β-functions (top curves) and dispersion. The horizontal axis is the distance in meters. QTEST denotes the quadrupole to be added to the line prior to the undulator.

A smaller β_{e^-} reduces ε_p while larger β_{e^-} reduces $\sigma_{p,hutch}$. The best compromise is around β_{e^-}= 60 horizontally and β_{e^-}=15 m vertically, with α_{e^-}= β_{e^-}/D.
Achieving exactly this desired combination of horizontal and vertical α_{e^-} and β_{e^-} requires four quadrupoles downstream of the chromatic correction section just upstream of the undulator. The present beamline has only one quadrupole. A second quadrupole will be installed in order to approach the desired optics. The electron optics with two quadrupoles is shown in Figure 9 with the resulting photon beam parameters shown in **Table 5**.

Table 5. Electron and photon beam envelope parameters

	Electron optics at center of undulator		*Resulting photon parameters at the hutch*	
	β_{e^-}(m)	α_{e^-}	ε_p (nm)	$\sigma_{p,hutch}$(mm)
Horizontal	26	0.18	1.1	0.65
Vertical	27	0.44	0.33	0.43

The only constraint on the electron optics downstream of the SPPS undulator is the requirement that most of the electrons reach the beam dump. A toroid at the beginning of the FFTB beamline and another at the end measure the transmission efficiency to the beam dump. If more than 20 percent of the beam is lost, the electron beam is automatically shut off to guard against high radiation levels outside the shielding. To ensure good transmission efficiency, a new quadrupole will be installed in the long straight section between the final vertically bending dipoles and the beam dump. This quadrupole will focus the vertical dispersion generated by the vertical dipoles, and reduce the vertical beam size approaching the dump. Without this quadrupole, the vertical dispersion at the 1.5 inch diameter collimator, PC8, would be 0.56 m, giving a ±3.4 % energy acceptance, which is marginal compared to the total energy spread of the electron beam (±3.5%, as shown in **Figure 5g**).

5. The radiation characteristics

This Section tabulates the main properties of the radiation. The simulations described in Section 3 indicate that, at full compression, the energy spread in the electron beam will be ~1.5 % (rms, see **Figure 5g**).
The calculations shown here are based on the parameters of **Table 4**: an undulator optimized for a fundamental energy of 8.3 keV. The observation parameters used in calculating the integrated spectral-angular flux are depicted in **Figure 10**. The use of angular units normalized to

$$\gamma^* = \gamma\left(1+\frac{K^2}{2}\right)^{-0.5} \qquad (4)$$

yields spectral flux distributions that, as functions of photon energy normalized to the fundamental, are invariant with respect to γ. In these units the quantity $\gamma^*\theta$ [rad] represents the angular radius of the far-field distribution for arbitrary values of γ.
The basic spectral performance of the undulator is graphically displayed in **Figures 11 and 12**. The aperture used in the calculations illustrated in **Figures 11** is defined by the angular aperture of the undulator duct and that of **Figure 12** by the emittance of the fundamental undulator harmonic. All the spectra were calculated using a rigorous formalism based on the Fourier transform, of the retarded vector potential[23]. In all the calculations insertion device fields with sinusoidal fields were assumed.
Figure 11 shows the photon flux of the first 11 harmonics, integrated over the angular aperture of the undulator duct. In **Figure 12** the photon flux, integrated over the undulator fundamental emission angle, is shown to extend over 1 MeV.

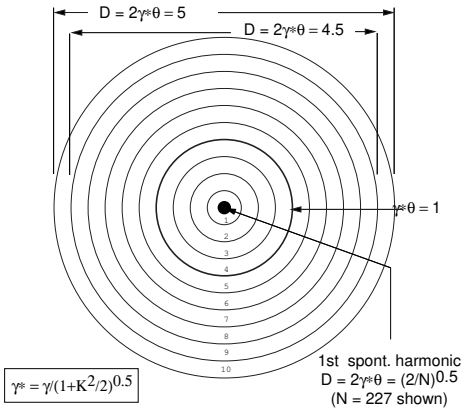

Figure 10. Radiation far-field target geometry in normalized angle space.

[23] R. Tatchyn. A. D. Cox, S. Qadri, "Undulator Spectra: Computer Simulations and Modeling," SPIE Proceedings No. 582, 47(1986).

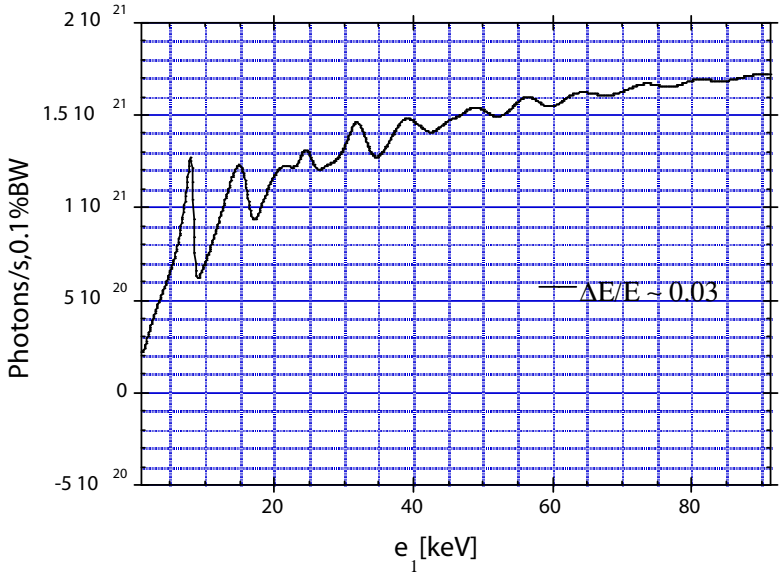

Figure 11. Full angle-integrated undulator spectrum through the 11th harmonic. The photon energy spread induced by the electron beam energy spread is 3% (rms).

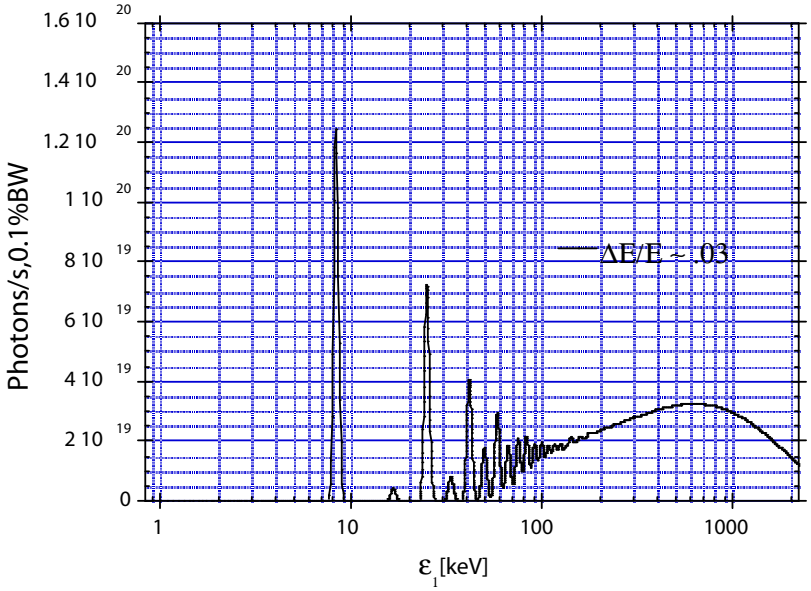

Figure 12. Undulator spectrum through the 120th harmonic integrated over the emittance-defined angular aperture of the fundamental.

Table 6. Some of the electron bunch parameters and the main properties of the spontaneous radiation are listed. The parameters of an alternative option of producing ultra-short pulses via time slicing with multi-layers (discussed in Section 2-i) are also listed in **Table 6** and are indicated with a *.

Parameters	*Values*	*Units*
Electron beam energy	28	Gev
Electron beam γ	54800	
Bunch charge	3.4	nC
Normalized horizontal bunch emittance	50	mm-mrad
Normalized vertical bunch emittance	10	mm-mrad
Horizontal emittance	$9.1x10^{-4}$	mm-mrad
Vertical emittance	$1.8x10^{-4}$	mm-mrad
Horizontal beta function in the undulator	26	m
Vertical beta function in the undulator	27	m
Beam current	30	kA
Electron bunch length, fwhm	80	fsec
Photon pulse length, fhhm	80	fsec
Time sliced photon pulse length, fwhm*	>80	fsec
Insertion device period	4.52	cm
Insertion device length	10	m
Insertion device K	6.0	
Insertion device natural vertical β	87	m
Repetition rate	30	Hz
Fundamental photon energy [keV]	8.3	
Peak Brightness	9.1×10^{24}	ph/s,mm^2,mr^2,0.1%bw
Average Brightness	2.2×10^{13}	ph/s,mm^2,mr^2,0.1%bw
Peak spectral flux	1.3×10^{21}	ph/s,0.1% bw, all angles
Average spectral flux	3.1×10^{9}	ph/s,0.1% bw, all angles
Output photons per pulse	1.0×10^{8}	ph/0.1% bw, all angles
Output photons/sliced pulse*,**	5.0×10^{6}	ph/0.1% bw, all angles
Coherent output photons per pulse	4000	ph/0.1% bw
Coherent output photons/sliced pulse*,**	200	ph/0.1% bw
Peak spontaneous radiation power	35.4	GW
Peak power density @200:1 foc., in 1% bw	1.9×10^{14}	W/cm^2

*Assuming a 0.64 % correlated rms electron energy chirp, a 0.03% uncorrelated rms electron energy spread, a 0.1% multiplayer bandwidth and an uncompressed bunch length of ~1.6 psec (fwhm).
**100% multilayer efficiency assumed

Power loading of SPPS optical elements

Although the peak power emitted by the SPPS insertion devices is in the several-hundred GW range, the average power is only on the order of 1 W. This reduces or eliminates the necessity for active cooling of optical elements. In **Table 7** the peak energy deposited per atom at normal incidence by the K=6.25 undulator is tabulated for selected materials spanning a broad range of Z. Due to the substantially broader angular spread of the radiation in comparison to the LCLS[5] the peak power damage is not expected to be an issue for the SPPS optics.

Table 7. Normal incidence peak energy loading for various materials at a distance of 34 m from the undulator end (location of the first optical element).

	Be	*C*	*Si*	*Au*
Density [gm-cm^{-3}]	1.848	2.1	2.33	19.3
Molecular Density [cm^{-3}] (x10^{22})	12.2	10.3	4.93	5.8
Und. Peak Power Density [W/cm^{-2}] (x10^{12})	3.3	3.3	3.3	3.3
Und. Peak Energy Loading [eV/atom]	7.4x10^{-8}	5x10^{-7}	1.64x10^{-5}	0.00053

6. Take-off optics and experimental area layout

It is proposed to extract the X-ray beam out of the FFTB tunnel and to set up an experimental hutch outside of the FFTB area. This choice is suggested by the limited space in the FFTB and by the desire to operationally decouple the experimental area from the electron beam to allow access to the experiment when the linac is being set up or during accelerator studies.
The geometry of the FFTB constrains the x-ray deflection to angles larger than about 8° with respect to the linac axis (see **Figure 13**).

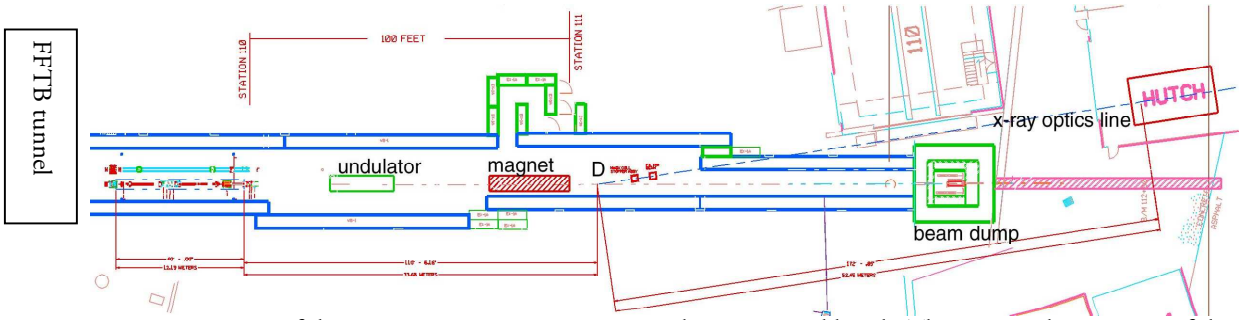

Figure 13. Layout of the x-ray optics transport system and experimental hutch. The magnet downstream of the undulator vertically deflects the electron beam onto the beam dump. The x-ray beam is deflected at the point indicated by "D" and taken to the experimental hutch outside the FFTB tunnel.

This deflection angle inhibits the use of either single or multiple grazing incidence mirrors. In the first case the incidence angle would be too large to transmit X-rays and in the second case the mirror array would need to be impracticably long. In view of this, optical schemes based on both multilayers and crystals for extracting the X-rays out along an approximately fixed axis are being investigated. In both cases the extraction point lies approximately 34 meters downstream of the undulator, at which location an existing chamber with the possibility of being modified to accommodate the extraction optics is located. In the present conceptual layout the extracted beam would exit the chamber at an angle of 8.5°. At this value it will intersect the FFTB tunnel wall for an interval of ~3 meters and then pass to the outside, skirting the FFTB radiation dump enclosure, and then proceed out for another ~12 meters before entering building 113. It is understood that this building will be torn down. A new building will be built in its place that will house the hutch.
The need for both crystal and multilayer extraction optics is determined by the desirability of providing continuous spectral tunability over a broad spectral range (**Figure 11**), say ~800 eV to ~25 keV. Given the cited beam line parameters, multilayer optics will be employed for energies between ~800 eV to ~13 keV, and crystals for energies of ~ 6 keV and higher. For operation above ~ 4 keV

the multilayer optics will be composed of tandem pairs of reflectors; below ~4 keV either tandem or single structures will be employed. The tandem reflectors are necessitated by practical lower limits on the periods at which multilayers of adequate quality (viz., reflectivity) can be fabricated. The takeoff energy will be tunable by using multilayers with relatively broad bandwidths and periods graded in the vertical direction. The tuning will be done by simple vertical displacements. The crystal takeoff optic will be implemented within a separate mechanism and will consist of at least two crystals. By varying the positional and angular coordinates of both elements the exit beam can be arranged to exit at approximately 8.5° and approximately parallel to the horizontal plane, but at a slightly different elevation than the multilayer exit beam. It should be noted that it will also be possible to use single crystals for extracting radiation out at exactly 8.5° and along a fixed horizontal axis, but these will only be capable of transmitting a spectrum of discrete energies and their harmonics.

Between the takeoff optics chamber and the FFTB inside wall a chamber containing one pair each of horizontal and vertical slits will be installed. This chamber will also be coupled to a pair of Personnel Protection System (PPS) stoppers which will be activated during access to the experimental hutch. The section of the beam line between the outside of the FFTB tunnel and the hutch will rest on standard support frames and will be shielded with modular concrete segments to satisfy radiation safety requirements.

7. Schedule and cost

The facility would be located in the Final Focus Test Beam (FFTB), in the area eventually occupied by the LCLS undulator. The advantage of starting the research in the FFTB is twofold: it is the most cost and time effective way to achieve sub-picosecond pulses and it allows to carry out accelerator studies that are important for the LCLS R&D, while providing a powerful source of spontaneous radiation for experiments.

The timeline of the project is shown in Figure 14. The project takes 17 months to complete construction and 2 months of commissioning. A more detailed scheduled is outlined in Appendix 1.

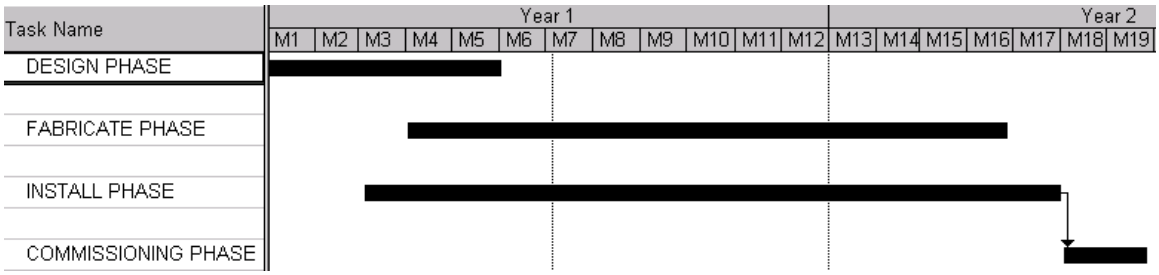

Figure 14. Design, construction and commissioning stages.

By a preliminary estimate, the construction cost of the SPPS is M$ 9.6, inclusive of 30% contingency. This cost (in thousand of dollars) is divided amongst the various components as follows:

Compressor and other magnets, electron beam instrumentation	658
Undulator	*1,551*
X-ray optics	397
Vacuum equipment	564
Controls, cabling, MPS/PPS, power supplies	*548*
Experimental hall, hutch, laser clean room	*664*
Laser for pump-probe experiments	*691*
Accelerator and undulator physics design, project management	*1,032*
Contigency (30%)	*1,832*
Indirect costs	*1,710*
Total	***9,649***

A more detailed breakdown of the cost is shown is shown in Appendix 2.

The staff needed during the construction phase (17 months) is as follows. The numbers represent the Full Time Equivalent over the 17 months construction period.

Engineering, design and inspection	*1.6*
Labor and technical support	*7.2*
Accelerator physics and undulator magnetic design	*3.0*
X-ray optics physics and beamline design	*1.0*
Project Management	*1.6*

The cost of running the facility has yet to be estimated, but it will take advantage of the fact that the linear accelerator (where most of the power consumption is) will be available because the rf is normally left on in between PEP-II fills.

*Acknowledgements:

This work is supported in part by the U.S. Department of Energy, Office of Basic Energy Sciences (contract number DE-AC03-76SF00515)

Appendix 1

Construction phase timeline

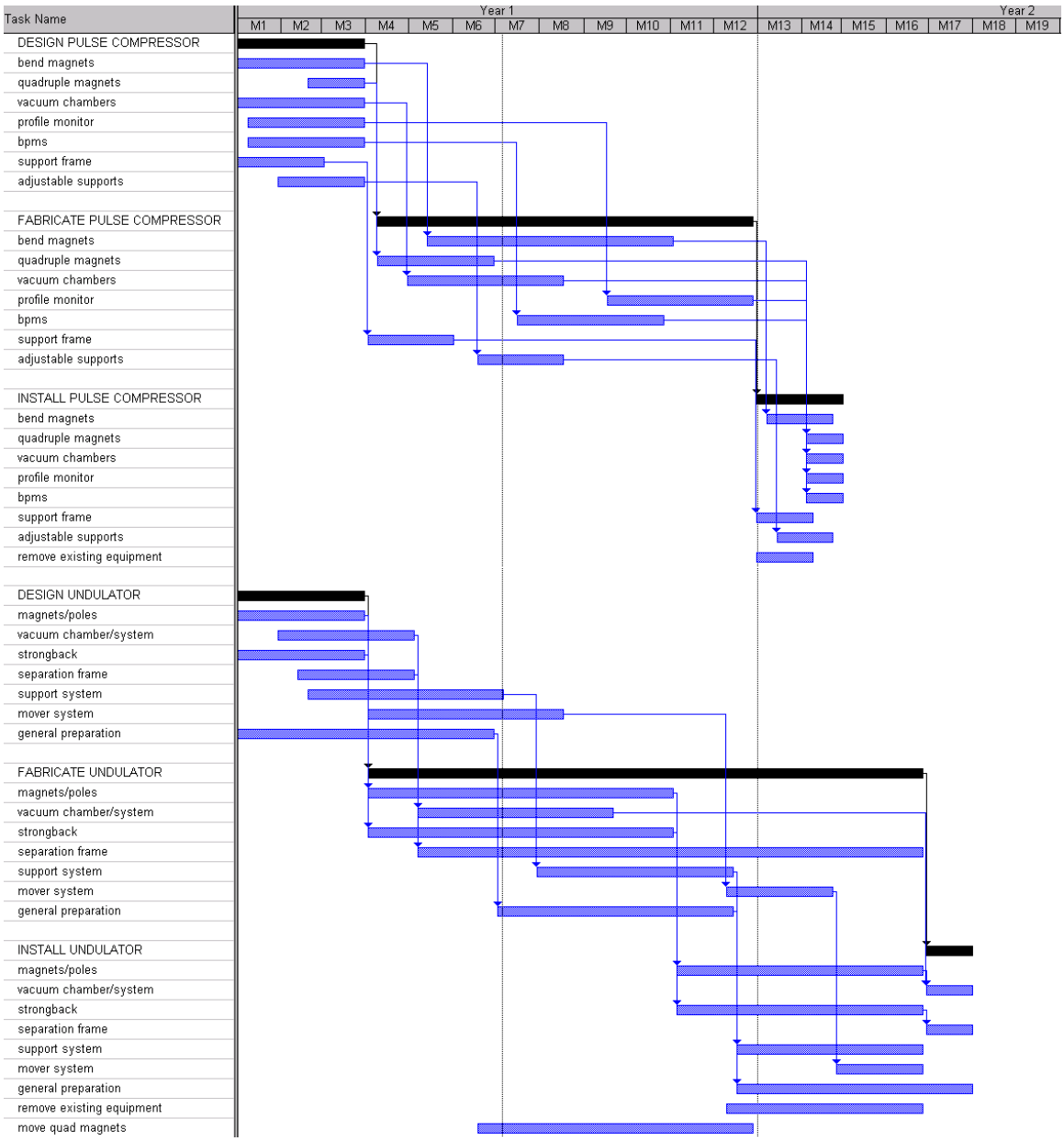

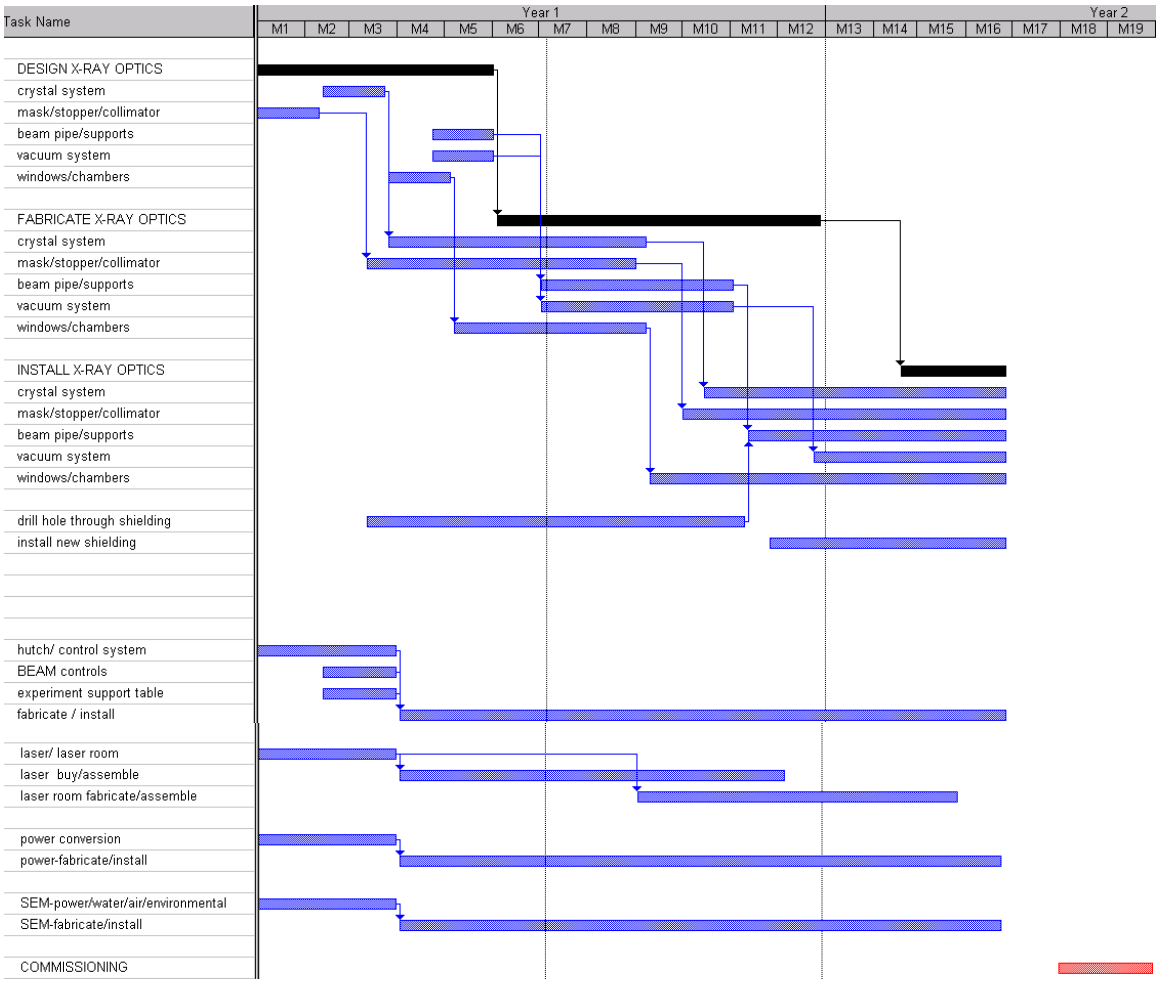
Task Name
Year 1
Year 2
M1
M2
M3
M4
M5
M6
M7
M8
M9
M10
M11
M12
M13
M14
M15
M16
M17
M18
M19
DESIGN X-RAY OPTICS
crystal system
mask/stopper/collimator
beam pipe/supports
vacuum system
windows/chambers
FABRICATE X-RAY OPTICS
crystal system
mask/stopper/collimator
beam pipe/supports
vacuum system
windows/chambers
INSTALL X-RAY OPTICS
crystal system
mask/stopper/collimator
beam pipe/supports
vacuum system
windows/chambers
drill hole through shielding
install new shielding
hutch/ control system
BEAM controls
experiment support table
fabricate / install
laser/ laser room
laser buy/assemble
laser room fabricate/assemble
power conversion
power-fabricate/install
SEM-power/water/air/environmental
SEM-fabricate/install
COMMISSIONING

Appendix 2

Breakdown of cost estimate

PROJECT: SPPS

		B&H									ED&I				
		MATERIAL				LABOR									
	ITEM	MEAS	# UNITS	UNIT COST	TOTAL	# UNITS	UNIT HRS	TOTAL HRS	$/HR	TOTAL	# UNITS	UNIT HRS	TOTAL HRS	$/HR	TOTAL
12	5 Quad magnets	ea	5	9,000	45,000	5	120	600	64	38,400			80	64	5,120
13	Quad supports	ea	2	2,000	4,000	2	40	80	64	5,120			60	64	3,840
14	bend magnets	ea	4	25,000	100,000	4	120	480	64	30,720			120	64	7,680
15	bend support stands	ea	4	5,000	20,000	4	120	480	64	30,720			240	64	15,360
16	bend support assemblies	ea	4	2,500	10,000	4	80	320	64	20,480			120	64	7,680
17	4 chambers	ea	4	11,000	44,000	4	200	800	64	51,200			240	64	15,360
18	BPM	ea	1	9,500	9,500	1	120	120	64	7,680			120	64	7,680
19	profile monitor	ea	1	17,000	17,000	1	480	480	64	30,720			160	64	10,240
20	BPM - PM supports	ea	2	2,000	4,000	2	60	120	64	7,680			60	64	3,840
21															
22	2 sextuple magnets	ea	2	12,000	24,000	2	200	400	64	25,600			16	64	1,024
23	Sextuple supports	ea	2	2,000	4,000	2	40	80	64	5,120			60	64	3,840
24	Quad/Sext stands	ea	4	1,500	6,000	4	120	480	64	30,720			80	64	5,120
25															
26	UND	ea		BID	900,000								160	64	10,240
27	UND strong back frame	ea	10	7,500	75,000	10	40	400	64	25,600			160	64	10,240
28	UND support assemblies	ea	10	2,000	20,000	10	80	800	64	51,200			160	64	10,240
29	UND mover support	ea	3	5,000	15,000	3	220	660	64	42,240			240	64	15,360
30	UND mover	ea	6	2,000	12,000	5	160	800	64	51,200			120	64	7,680
31	Newport tables & vibe eq	bid	1		55,000	2	240	480	64	30,720			80	64	5,120
32	heat treat / finish		20	300	6,000	20	8	160	64	10,240			80	64	5,120
33	UND beam pipe	ea	4	3,000	12,000	4	120	480	64	30,720			120	64	7,680
34	UND assembly jigs	ea	3	5,000	15,000	3	80	240	64	15,360			160	64	10,240
35	2 UND Quad magnets	ea	2	9,000	18,000	2	120	240	64	15,360			16	64	1,024
36	Quad supports	ea	2	2,000	4,000	2	40	80	64	5,120			60	64	3,840
37	temp control system	bid			25,000					5,000			40	64	2,560
38	UND alignment				1,000	3	120	360	56	20,160			20	56	1,120
39															
40	crystal	ea	5	5,000	25,000	5	60	300	64	19,200			40	64	2,560
41	crystal support/mover	ea	1	15,000	15,000	1	220	220	64	14,080			80	64	5,120
42	crystal fixture	ea	2	12,000	24,000	2	220	440	64	28,160			40	64	2,560
43	Be windows	cooled	4	4,500	18,000	4	40	160	64	10,240			20	64	1,280
44	crystal chamber	ea	1	7,500	7,500	1	120	120	64	7,680			60	64	3,840
45	monochromator	refurbish			10,000	1	120	120	55	6,600					
46	mask/stopper/collimator	full assy	1	69,000	69,000	1	480	480	64	30,720			20	64	1,280
47	support system		1	6,500	6,500	1	220	220	64	14,080			40	64	2,560
48	stopper shielding hutch		1	8,000	8,000	1	320	320	64	20,480			30	64	1,920
49	filter/support	graphite	1	25,500	25,500	1	220	220	64	14,080			40	64	2,560
50															
51	beam pipe	10 ft	10	2,000	20,000	10	100	1,000	64	64,000			40	64	2,560
52	supports		12	1,000	12,000	12	40	480	64	30,720			40	64	2,560
53	enclosure	concret	1	20,000	20,000	1	200	200	64	12,800			40	64	2,560
54	Ion pump	30L	9	4,600	41,400	9	20	180	64	11,520			30	64	1,920
55	NEG pump assy.	ea	7	8,500	59,500	7	120	840	64	53,760			30	64	1,920
56	turbo pump	ea	2	8,000	16,000	2	80	160	64	10,240			30	64	1,920
57	vacuum valve	ea	3	7,500	22,500	3	120	360	64	23,040			20	64	1,280
58	vac flanges/fittings/hdw	ea	50	200	10,000	50	8	400	64	25,600			40	64	2,560
59	bellows	ea	20	500	10,000	20	20	400	64	25,600			40	64	2,560
60	drift sections	ea	7	500	3,500	7	10	70	61	4,270			40	64	2,560
61	pump ps	ea	5	2,600	13,000	5	3	15	61	915			80	64	5,120
62	bellows/manifold	ea	15	750	11,250	15	8	120	61	7,320			40	64	2,560
63	cold cath & pirani gauges	set	3	750	2,250	3	8	24	61	1,464			20	64	1,280
64	gauge controllers/HPS	ea	3	1,900	5,700	3	4	12	61	732			20	64	1,280
65	hot filament gauge	ea	3	450	1,350	3	4	12	61	732			20	64	1,280
66	multigauge controller	ea	3	1,900	5,700	3	3	9	61	549			40	64	2,560
67															
68	cable trays				10,000	2	80	160	50	8,000			0		0
69	hardware removal				5,000	2	120	240	64	15,360			0		0
70	cable plant				7,500	2	120	240	50	12,000			0		0
71	mag power supplies				150,000			0		20,000			0		20,000
72	controls harware/instal				15,000			0		15,000			0		0
73	alignment	gen. eqt			3,000	1	220	220	56	12,320			40	64	2,560
74	plumbing				10,000	1	220	220	42	9,240			40	64	2,560
75	MPS/PPS	X-ray			23,000	2	220	440	50	22,000			80	64	5,120
76															
77	experimental hall	complete			500,000			0		0			0		0
78	hutch	11.20	1	25,500	25,500	1	220	220	55	12,100			40	64	2,560
79	laser room				100,000	2	220	440	55	24,200					

80															
81	control console	complete (electr&motion)			40,000	4	120	480	64	30,720			60	64	3,840
82	LASER system	complete			500,000			0		0					
83	LASER support equip.				100,000										
84	experimental table	refurbish			10,000	1	120	120	55	6,600					
85															
86	ENGINEERING (MAG/VAC/etc.)										1	250	250	64	16,000
87	DESIGN (layout/etc.)										1	250	250	56	14,000
88	MECHANICAL FAB							80	79	6,320			0		0
89	QC							320	56	17,920			0		0
90	PRECISION ASSEMBLY							220	64	14,080			0		0
91	PLATING & CLEANING							120	134	16,080			0		0
92	WELDING							60	64	3,840			0		0
93	POWER CONVERSION	fftb/hutch			20,000			220	41	9,020	1	120	120	64	7,680
94	SEM	air/water/power			20,000			220	65	14,300	1	120	120	64	7,680
95	PHYSICS DESIGN									0	3	3,000	9,000	64	576,000
96	BEAM LINE/EXPERIMENT COORD.									0	1	3,000	3,000	56	168,000
97	PROJECT MANAGEMENT									0	2	2,250	4,500	64	288,000
98	MECHANICAL TECHS							220	64	14,080			0		0
99	**SUBTOTAL**				3,447,150					1,308,842					1,351,408
100	**30% CONTINGENCY**				1,034,145					392,653					405,422
101	**SUPPORT COST**				430,204					629,553					650,027
102															
103	TOTAL B&H				$7,242,547										
104	TOTAL ED&I				$2,406,858										
105	**PROJECT TOTAL**				**$9,649,405**										